Statistical mechanics of two-dimensional shuffled foams: Geometry-topology correlation in small or large disorder limits

Marc Durand,[1,*] Andrew M. Kraynik,[2] Frank van Swol,[3,4] Jos Käfer,[5,†] Catherine Quilliet,[6,‡] Simon Cox,[7] Shirin Ataei Talebi,[6,‡] and François Graner[1,§]

[1]*Matière et Systèmes Complexes (MSC), 10 rue Alice Domon et Léonie Duquet, 75205 Paris Cedex 13, France*
[2]*Division of Chemistry and Chemical Engineering, California Institute of Technology, Pasadena, California 91125, USA*
[3]*Sandia National Laboratories, P.O. Box 5800, Albuquerque, New Mexico 87185, USA*
[4]*Chemical and Nuclear Engineering Department, The University of New Mexico, Albuquerque, New Mexico 87106, USA*
[5]*Laboratoire de Biométrie et Biologie Evolutive, 43 Boulevard du 11 Novembre 1918, 69622 Villeurbanne Cedex, France*
[6]*Laboratoire Interdisciplinaire de Physique, Boîte Postale 87, 38402 Martin d'Hères Cedex, France*
[7]*Departments of Mathematics and Physics, Aberystwyth University, Aberystwyth SY23 3BZ, United Kingdom*

(Received 2 April 2014; published 19 June 2014)

Bubble monolayers are model systems for experiments and simulations of two-dimensional packing problems of deformable objects. We explore the relation between the distributions of the number of bubble sides (topology) and the bubble areas (geometry) in the low liquid fraction limit. We use a statistical model [M. Durand, Europhys. Lett. **90**, 60002 (2010)] which takes into account Plateau laws. We predict the correlation between geometrical disorder (bubble size dispersity) and topological disorder (width of bubble side number distribution) over an extended range of bubble size dispersities. Extensive data sets arising from shuffled foam experiments, SURFACE EVOLVER simulations, and cellular Potts model simulations all collapse surprisingly well and coincide with the model predictions, even at extremely high size dispersity. At moderate size dispersity, we recover our earlier approximate predictions [M. Durand, J. Kafer, C. Quilliet, S. Cox, S. A. Talebi, and F. Graner, Phys. Rev. Lett. **107**, 168304 (2011)]. At extremely low dispersity, when approaching the perfectly regular honeycomb pattern, we study how both geometrical and topological disorders vanish. We identify a crystallization mechanism and explore it quantitatively in the case of bidisperse foams. Due to the deformability of the bubbles, foams can crystallize over a larger range of size dispersities than hard disks. The model predicts that the crystallization transition occurs when the ratio of largest to smallest bubble radii is 1.4.

DOI: 10.1103/PhysRevE.89.062309 PACS number(s): 83.80.Iz, 02.70.Rr

I. INTRODUCTION

Bubble monolayers with low liquid content, in which bubbles tile the plane without gaps or overlaps, are model systems for experiments and simulations of two-dimensional (2D) packing problems with deformable objects. In such a quasi-two-dimensional foam, the average bubble size is determined by the total number of bubbles. The average bubble side is determined by Euler's theorem and is equal to 6. Hence what distinguishes two foams are their disorders [1,2]. The geometrical disorder is the relative width of the bubble size distribution; it is fixed by the repartition of gas between bubbles, and it plays a role in a foam's mechanical properties [3]. The topological disorder is the relative width of the bubble side number distribution; it is determined by the past history of the foam, and it plays a role in foam coarsening [4].

Statistically, within a given bubble configuration, a relatively large bubble has more neighbors than a smaller one. Thus the geometrical disorder affects the topological disorder; experiments and simulations suggest that both measures of disorder are correlated [5]. Understanding this geometry-topology correlation requires a statistical description of foam structure; this is a challenge [6]. Existing models are based on energy minimization only [7,8], entropy only [9–15], or a balance of both energy and entropy to determine a free energy using a statistical mechanics approach: de Almeida and Iglesias [16] proposed a detailed prediction of foam structure and predict the distributions of bubble area (in cases where it is supposed to be free, for instance, in the self-similar coarsening regime [2]) or topology. One more recent attempt describes bubbles by their size, irrespective of their shape, and predictions are based upon a packing of hard disks around which polygons are drawn [17].

Conversely, one of us has proposed a statistical approach in which a space-filling constraint (curvature sum rule [1]) replaces an energetic constraint [18]. It allows, in a mean-field approximation, to determine the probability distribution of the number of sides of a bubble of given area; it thus applies in principle to a foam which has any given bubble area distribution. Using a mean-field approximation valid at moderate geometrical disorders, we have solved this model analytically and successfully compared its predictions with experiments and simulations, without adjustable parameters [19].

Here, we further develop that work. Section II describes the model. Section III shows that, without approximation, this model predicts the foam topological disorder for a very large range of dispersities. Section IV successfully compares it, again without adjustable parameters, with the preceding experiments and simulations complemented by new simulations at even higher dispersity. Section V investigates in detail the topological ordering at very low dispersity.

*UMR 7057 CNRS and Université Paris Diderot; marc.durand@univ-paris-diderot.fr
†UMR 5558 CNRS and Université Lyon I.
‡UMR 5588 CNRS and Université Grenoble I.
§UMR 7057 CNRS and Université Paris Diderot.

II. MODEL

A. Principle

Our model is based on the ideas introduced in Ref. [18], which we now briefly recall. For each given bubble, we denote by A its area, P its perimeter, and n its number of sides. In what follows we largely use its effective radius $R = \sqrt{A/\pi}$, i.e., the radius of the circle which has the same surface area, because it correlates well with its number of sides (see Fig. 10 below). Finally we denote by $e = P/\sqrt{A} = P/(R\sqrt{\pi})$ its elongation.

At low liquid fraction, 2D bubbles are polygons with curved sides. Their sides have a uniform line tension, so that the foam energy is proportional to the sum of bubble perimeters. Bubbles decrease their energy by decreasing their contact perimeter with their neighbors. Their shapes are locally governed by the following Plateau laws [2,20]: (i) Each side is a film separating two bubbles; its curvature is determined by the difference of pressure between these two bubbles: thus each side has constant curvature, that is, it is an arc of circle. (ii) The sides meet in threes at 120° angles.

Due to the simplicity of these local laws, a bubble has a rather regular shape. Despite the existence of correlations between the number of sides of neighboring bubbles [1,2,21,22], it happens that the correlations between the size and number of sides of a bubble are close to those of a regular bubble (i.e., with sides of same length and curvature) [2,8,23]. Therefore, the elongation e is always close to the average elongation of a regular bubble, which in turn is close to that of a hexagon, whatever n. In practice e is close to $\bar{e} \simeq 2^{3/2}3^{1/4} \simeq 3.72$:

$$P \simeq \bar{e}\sqrt{\pi}R. \tag{1}$$

Thus for a given area distribution, the total foam energy is almost fixed. Within a macrostate, the set of microstates is defined as the set of all accessible local energy minima: we assume they all have the same probability, and that energy does not play any role of selection between microstates. We now discuss the extensive variables that define a macrostate.

In a shuffled foam (see Sec. IV for discussion of this notion), bubbles can undergo topological changes (called "T1 processes" [1,2,24]) in which they change neighbors, without changing their area, and thus swap sides and side numbers. We define a bubble curvature κ as the sum of the algebraic curvatures of its sides. We count the curvature of a bubble side as positive if the center of curvature is outside the bubble. In the same mean-field approximation, where neighbor correlations are disregarded and every bubble is surrounded by a homogeneous and isotropic foam, the 2D Gauss-Bonnet theorem implies that each side of an n-sided bubble has on average a curvature $(n-6)\pi/(3P)$ [2,8]. Hence

$$\kappa = \frac{n(n-6)\pi}{3P} \approx \frac{\sqrt{\pi}}{3\bar{e}R}n(n-6), \tag{2}$$

for $n \geqslant 2$ ($n = 1$ is not a stable configuration as the two above Plateau laws cannot be simultaneously satisfied). For $n = 3$, κ reaches its lower bound, which is negative: $\kappa_{\min} = -3\sqrt{\pi}/(\bar{e}R)$. On the other limit, at large n, κ is positive and can be arbitrarily large.

Each T1 contributes to the redistribution between neighboring bubbles of two quantities: the curvature and the number of sides. That is, during a T1, two bubbles lose a side and two other bubbles gain one side, while the sum of n over the four bubbles involved, and hence the total number $N_s = \sum n$ of sides in the foam, remains constant. Similarly, the sides created or destroyed during a T1 have a curvature contributing positively to a bubble and negatively to its neighbor. Thus the total curvature is strictly conserved. Since, in the mean-field approximation, the curvature of a bubble is related to its number of sides [Eq. (2)], the sum of κ over the four bubbles involved in the T1 also remains constant. A foam's macrostate is then defined by its total curvature κ_{tot} and total number of sides N_s, which are constant during any shuffling from one microstate to another. We denote by $\langle\cdot\rangle$ the average over all bubbles in a foam. For a very large foam ($N \to \infty$), the constraint of space filling sets the values [2,24,25]:

$$\langle\kappa_{\text{tot}}\rangle \to 0, \quad \langle N_s\rangle \to 6N. \tag{3}$$

B. Grand-canonical description

Equations (3) provide an implicit relation between the distributions of bubble sizes and side numbers. We thus turn to a grand-canonical description: for a given bubble with size R, the rest of the foam constitutes a reservoir of sides and curvature, exchanged through T1s. We denote by $p(R)$ the bubble size distribution, and $p(n)$ the side number distribution. The probability $p_R(n)$ for a bubble with size R to have n sides (conditional side number distribution) is

$$p_R(n) = \frac{1}{\xi(R)}\exp\left[-\frac{\beta\sqrt{\pi}}{3\bar{e}R}n(n-6) + \mu n\right], \tag{4}$$

where the partition function of the bubble is

$$\xi(R) = \sum_{n\geqslant 2}\exp\left[-\frac{\beta\sqrt{\pi}}{3\bar{e}R}n(n-6) + \mu n\right]. \tag{5}$$

Here β^{-1} and $\mu\beta^{-1}$ are analogous to the "temperature" of the reservoir of curvature, and the "chemical potential" of the reservoir of sides, respectively [26]. Their values are unambiguously related to the mean values of κ_{tot} and N_s through

$$\langle\kappa_{\text{tot}}\rangle = -\frac{\partial \ln \Xi}{\partial\beta}, \quad \langle N_s\rangle = \frac{\partial \ln \Xi}{\partial\mu}, \tag{6}$$

where Ξ is the partition function of the entire foam, defined as

$$\ln \Xi = N\int_0^\infty p(R)\ln\xi(R)dR. \tag{7}$$

Combining Eqs. (3) and (6) yields, in the limit of a large foam, the following system of equations:

$$\frac{\partial \ln \Xi}{\partial\beta} = 0, \quad \frac{\partial \ln \Xi}{\partial\mu} = 6N. \tag{8}$$

Solving Eqs. (8) yields the values of β and μ.

III. PREDICTIONS

For a perfectly monodisperse foam, an exact analytical resolution of Eqs. (8) is possible and, as expected, yields only six-sided bubbles [18]. Otherwise, the exact resolution of Eqs. (8) is more difficult. In Ref. [19] we derived analytical predictions, using approximations valid for a foam with

moderate polydispersity. We now want to extend this approach to a wider range of dispersities (Sec. III A) and compare it with the numerical resolution of the equations (Sec. III B).

A. Analytical resolution

Let us first introduce notation to simplify Eqs. (4) and (5). By defining

$$\widetilde{\beta} = \frac{\sqrt{\pi}}{3\bar{e}}\,\beta = 0.1587\beta \tag{9}$$

we can rewrite Eq. (4) as

$$p_R(n) = c(R)\exp\left[-\frac{(n-\bar{n}(R))^2}{2\sigma^2}\right], \tag{10}$$

with $\bar{n}(R)$ and $\sigma(R)$ defined by

$$\bar{n}(R) = 3 + \frac{\mu R}{2\widetilde{\beta}}, \quad \sigma^2(R) = \frac{R}{2\widetilde{\beta}}, \tag{11}$$

and the normalization prefactor given by

$$c(R) = \frac{1}{\xi(R)}\exp\left[\frac{\widetilde{\beta}}{R}\,\bar{n}^2(R)\right]. \tag{12}$$

Calculating $\xi(R)$ requires that we calculate the series $\sum_{n\geqslant 2}\exp[-(n-\bar{n}(R))^2/(2\sigma^2)]$ which defines $c(R)$ [Eq. (10)].

The terms of this series naturally suggest to approximate it, perhaps crudely, by a Gaussian integral. Although n is an integer larger than 2, we replace it by a real number that varies continuously from $-\infty$ to ∞. This amounts to approximating $c(R)^{-1}$ as

$$\frac{1}{c(R)} \approx \int_{-\infty}^{\infty}\exp\left[-\frac{\widetilde{\beta}}{R}(n-\bar{n}(R))^2\right]dn. \tag{13}$$

Within this approximation, $\bar{n}$ and σ represent the average and the standard deviation of the Gaussian law. Using Eqs. (12) and (13) we immediately obtain the partition function,

$$\xi(R) \approx \exp\left[\frac{\widetilde{\beta}\bar{n}^2(R)}{R}\right]\sqrt{\frac{\pi R}{\widetilde{\beta}}}, \tag{14}$$

and, through Eqs. (8), we solve for β (or $\widetilde{\beta}$) and μ:

$$\frac{1}{\beta} = \frac{6\sqrt{\pi}}{\bar{e}}\left(\left\langle\frac{1}{R}\right\rangle - \frac{1}{\langle R\rangle}\right), \tag{15}$$

$$\frac{1}{\mu} = 3\left(\langle R\rangle\left\langle\frac{1}{R}\right\rangle - 1\right). \tag{16}$$

As a first product of the calculation, we obtain the average side number for a given bubble size:

$$\bar{n}(R) \simeq 3\left(1 + \frac{R}{\langle R\rangle}\right). \tag{17}$$

This predicts a linear correlation between the geometry and topology of individual bubbles.

Second, we obtain the average of the square of the side number:

$$\langle n^2\rangle = \int_0^{\infty}\frac{p(R)}{\xi(R)}\,\frac{\partial^2\xi}{\partial\mu^2}\,dR. \tag{18}$$

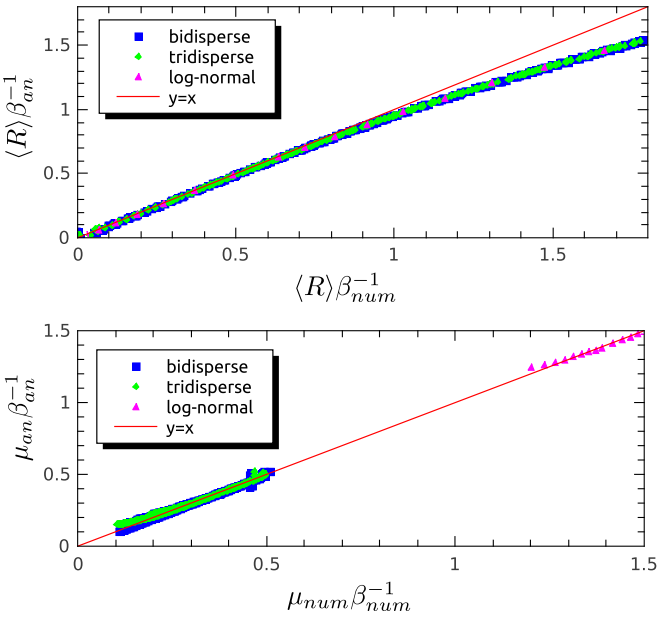

FIG. 1. (Color online) Analytical approximation [Eqs. (15) and (16)] vs numerical solution of Eqs. (8). Each point corresponds to a different foam with bidisperse, tridisperse, or log-normal distribution of bubble areas. Top: effective temperature β^{-1}, rescaled by the averaged bubble radius. Bottom: effective chemical potential $\mu\beta^{-1}$. The solid red line $y = x$ is a guide for the eye.

The topological disorder $\Delta n/\langle n\rangle = \sqrt{\langle n^2\rangle - \langle n\rangle^2}/\langle n\rangle$ can then be calculated, and expressed in terms of the characteristics of the size distribution:

$$\left(\frac{\Delta n}{\langle n\rangle}\right)^2 = \frac{1}{4}\left(\langle R\rangle\left\langle\frac{1}{R}\right\rangle + \frac{\langle R^2\rangle}{\langle R\rangle^2} - 2\right). \tag{19}$$

The right-hand side (rhs) of Eq. (19) defines a new parameter which characterizes the size disorder:

$$\mathcal{D} = \frac{1}{2}\sqrt{\langle R\rangle\langle R^{-1}\rangle + \langle R^2\rangle\langle R\rangle^{-2} - 2}, \tag{20}$$

i.e.,

$$4\mathcal{D}^2 = \langle R\rangle\left\langle\frac{1}{R}\right\rangle - 1 + \left(\frac{\Delta R}{\langle R\rangle}\right)^2. \tag{21}$$

B. Numerical resolution

We compare the analytical expressions [Eqs. (15) and (16)] with the numerical solution of Eqs. (8) for the following distributions of bubble areas: bidisperse, tridisperse, and log-normal. Figures 1 and 2 show that the analytical expressions are very good approximations in a range which is much larger than in Ref. [19]. At larger disorder, the analytical expressions are valid as long as $\langle R\rangle\beta^{-1} \lesssim 1$ and $\mathcal{D}^2 \lesssim 0.4$. At smaller disorder, the analytical expressions are valid down to the crystallization transition, which we now study in detail.

C. Order-disorder transition

For clarity, in Fig. 3 only two bidisperse foams extracted from Fig. 2 are shown. We observe (i) crystallization (only six-sided cells) of foams with low dispersity, (ii) a range

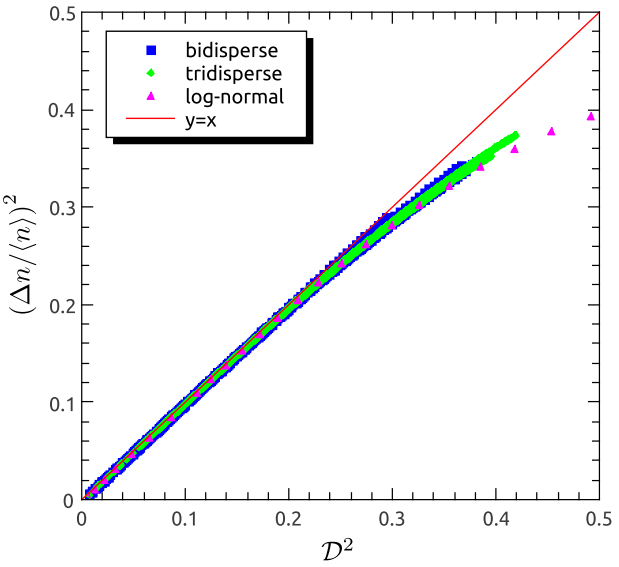

FIG. 2. (Color online) Topological disorder vs geometrical disorder parameter $\mathcal{D}$: comparison between numerical solution of Eqs. (8) (symbols) with the analytical approximation [Eq. (19)] (solid red line) for foams with bidisperse, tridisperse, and log-normal distributions of bubble areas. Each point corresponds to a different foam. Abscissa is the rhs of Eq. (19), defined in Eqs. (20) and (21).

of "forbidden" values of topological disorders (gap), and (iii) good agreement between analytics and numerics above the crystallization threshold.

Crystallization, which implies ordering (vanishing topological disorder), occurs even at finite geometrical disorder:

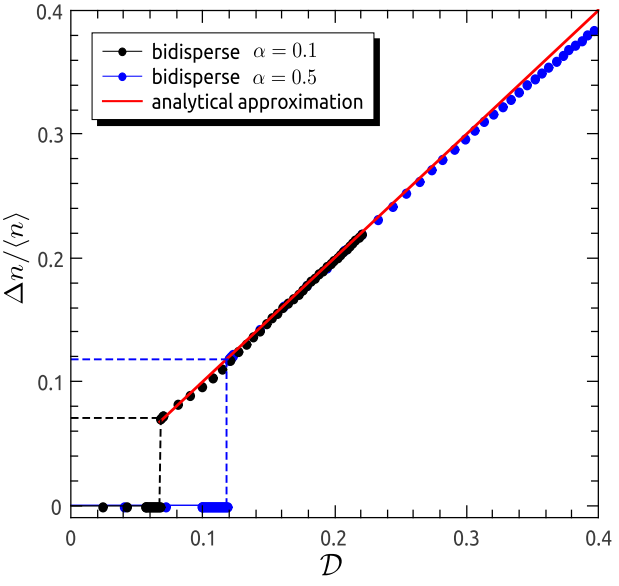

FIG. 3. (Color online) Comparison between numerical resolution of the equations of the model and their analytic approximation for two bidisperse foams with different fractions of small bubbles α, extracted from Fig. 2. Black dots, $\alpha = 0.1$; blue dots, $\alpha = 0.5$; solid red line, analytic approximation of the model [Eqs. (19) and (20)]. The dashed lines indicate the coordinates of the respective crystallization thresholds predicted by Eqs. (25) and (32).

all bubbles are hexagons although their areas differ slightly. This is simply due to the fact that the number of sides is an integer. The topological disorder is nonzero only when the foam contains bubbles with $n \neq 6$ sides, which implies a discontinuous transition. Points corresponding to the crystallized configurations are below the $y = x$ line in Fig. 3.

Although mean-field approximations are seldom appropriate for describing phase transitions, we can estimate the threshold at which the order-disorder transition takes place, that is, for the value of geometrical disorder at which our equations admit a solution with at least one nonhexagonal bubble. In the side number distribution [Eq. (10)], $n = 6$ is the dominant term, followed by $n = 5$ and 7. More precisely, since $\bar{n}(R)$ is an increasing function of R, large bubbles have six or seven sides only, and small bubbles have five or six sides only. Thus, just at the transition, at least one small bubble is five-sided and one large bubble is seven-sided: they appear simultaneously in order to preserve the average $\langle n\rangle = 6$. The following argument is valid for any shape of bubble size distribution, but we present it first for the bidisperse case, which is easier to explain.

Consider a bidisperse foam, which mixes two populations of bubbles with different sizes. We denote by R_s the radius of small bubbles, α their proportion, and by R_l and $1-\alpha$ for the large bubbles. The size ratio is $r = R_l/R_s > 1$. We introduce the simplified notation $p_n^s = p_{R_s}(n)$ and $p_n^l = p_{R_l}(n)$ for the proportions of n-sided small and large bubbles. Below the transition, the proportions p_6^s and p_6^l are one; all other proportions are zero. Above the transition, the proportions p_5^s and p_7^s are finite but small, while p_6^s and p_6^l slightly decrease accordingly. Normalization implies

$$p_5^s + p_6^s = 1, \quad p_6^l + p_7^l = 1. \tag{22}$$

With this notation, and using Eq. (2), just above the transition Eqs. (3) become

$$\alpha \, \frac{5}{R_s} \, p_5^s = (1-\alpha) \, \frac{7}{R_l} \, p_7^l, \tag{23}$$

$$\alpha \, p_5^s = (1-\alpha) \, p_7^l. \tag{24}$$

Dividing Eq. (23) by Eq. (24) indicates that the transition occurs for a critical large-to-small size ratio of

$$r_c = \tfrac{7}{5} = 1.4. \tag{25}$$

Figure 4 shows that the prediction of Eq. (25) is in excellent agreement with the numerical solution of the model, which yields $r_c \simeq 1.4$ for any proportion α of small bubbles.

In fact, this result is not sensitive to the details of the model. It does not depend on the respective proportions of bubbles, or even on the foam being bidisperse: in a well-shuffled foam with any bubble size distribution, the order-disorder transition occurs when there exist at least two bubbles with sizes in a ratio $\geqslant 1.4$.

This crystallization threshold sheds light on the peculiar behavior investigated by Aste and Sherrington [27]. They considered 2D foams from a purely topological point of view, characterizing bubbles only by their lists of neighbors (and not by their size or shape). They simulated large numbers of bubble rearrangements in such foams and observed a "glass

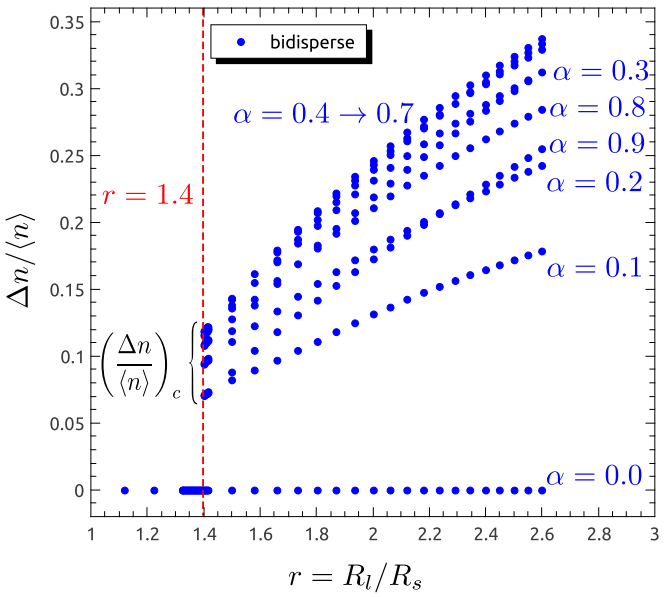

FIG. 4. (Color online) Topological disorder vs large-to-small-radius ratio $r = R_l/R_s$ for bidisperse foams with various small bubble proportions α.

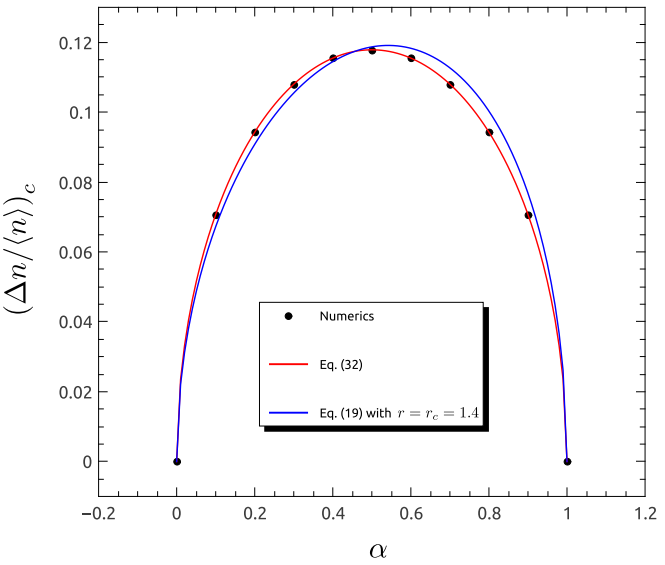

FIG. 5. (Color online) The value of topological disorder at the crystallization threshold vs the proportion of small bubbles. Dots, numerical resolution; red line, prediction from the model for a bidisperse foam [Eq. (32)]; blue line, value obtained by the analytical approximation [Eq. (19)] taken for a bidisperse foam with bubble size ratio $r = r_c = 1.4$.

transition" as their parameter $\beta_{\rm AS}$ reaches the critical value $\simeq$2.4. This parameter corresponds, in our notation, to

$$\beta_{\rm AS} = \frac{\widetilde{\beta}}{R} = \frac{\langle R\rangle}{18R}\,\frac{1}{\langle R\rangle\langle R^{-1}\rangle - 1}. \tag{26}$$

Taking $R = R_s$ and $\alpha = 0.5$, we obtain at $r = r_c$ the value 2.33 for this parameter, which is close to Aste and Sherrington's value.

It is interesting to compare our value of $r_c = 1.4$ [Eq. (25)] with that of hard disks, where the determination of r_c is sensitive to the definition of neighborhood. Hamanaka and Onuki [28] define two Lennard-Jones particles as neighbors if their distance is less than 1.5 times the Lennard-Jones distance; with this definition they find a transition at $r_c \approx 1.17$–1.2 [28].

Taking a stricter definition, as for instance in the case of perfectly rigid hard disks, would result in an even smaller value of r_c.

This shows that, due to their deformability, bubbles can accommodate more dispersity than hard disks while all bubbles remain six-sided. This is reminiscent of the "kissing problem": while a hard disk can have at maximum only 6 identical neighbors, a deformable bubble can accommodate 12 neighbors of the same area [29].

D. Disorder at crystallization threshold

For a bidisperse foam, the proportions of five-, six-, and seven-sided bubbles at the transition are easily calculated, since Eq. (4) gives

$$\frac{p_5^s}{p_6^s} = \exp\left(\frac{5\widetilde{\beta}}{R_s} - \mu\right), \tag{27}$$

$$\frac{p_7^l}{p_6^l} = \exp\left(-\frac{7\widetilde{\beta}}{R_l} + \mu\right). \tag{28}$$

Multiplying Eq. (27) by Eq. (28) and using Eq. (25) shows that, at the transition ($r = r_c$),

$$p_5^s\, p_7^l = p_6^s\, p_6^l. \tag{29}$$

Solving the four Eqs. (22), (24), and (29) for the four unknowns p_5^s, p_6^s, p_6^l, and p_7^l yields

$$p_5^s = p_6^l = 1 - \alpha, \quad p_6^s = p_7^l = \alpha. \tag{30}$$

At the transition, Δn can be calculated:

$$(\Delta n)^2 = \alpha p_5^s + (1-\alpha)p_7^l = 2\alpha(1-\alpha), \tag{31}$$

so that the critical topological disorder value $(\Delta n/\langle n\rangle)_c$ at the transition is

$$\left(\frac{\Delta n}{\langle n\rangle}\right)_c = \frac{\sqrt{2\alpha(1-\alpha)}}{6}. \tag{32}$$

Figure 5 compares this expression with the numerical solution. The values obtained confirm that the approximation is very good up to the crystallization transition. We also report on this figure the critical value obtained from the approximate solution [Eq. (19)] for a bidisperse distribution with bubble size ratio $r = r_c = 1.4$. Despite a slight asymmetry in the latter prediction, the agreement is surprisingly good, given that Eq. (19) relies on a mean-field approximation and treats the integer n ($n \geqslant 2$) as if it could take all real values.

The details of the model and of the bubble size distribution do play a role to estimate the proportions of five-, six-, and seven-sided bubbles at the transition. For an arbitrary bubble size distribution, what matters are the tails at small and large sizes. More precisely, in Eq. (32) the number α should be

replaced by the proportion of bubbles, in these tails, which have sizes in a ratio $\geqslant 1.4$.

IV. TESTS

The notion of "shuffling" is empirically defined as "having enough T1 processes per bubble to forget about the foam's initial preparation" [5,16], that is, to remove both residual trapped stresses and spurious correlations. Numerical simulations and theoretical analyses have made precise the conditions under which the initial preparation can really be forgotten for a foam under shear; they have shown that perfect shuffling is seldom reached in practice but can be well approximated by cycles of shear along all directions, with an amplitude that is at first significantly larger than the yield strain, and then progressively decreases [30,31].

Experiments were performed with 2D foams with a small fraction of water (rather "dry" foams). Simulations were performed in the completely dry limit. The distributions of areas were either bidisperse or polydisperse [in simulations we used normal (Potts), Poisson (SE1), or log-normal (SE2) distributions, as described below], with relative width $\Delta A/\langle A\rangle = \sqrt{\langle A^2\rangle - \langle A\rangle^2}/\langle A\rangle$ ranging from 0 to 6.46. Most experiments and simulations used here have already been presented in Ref. [19].

Briefly, in experiments (Fig. 6), a bubble monolayer of up to $N = 2700$ bubbles is confined at the air-water interface by a glass plate [32]. The foam is enclosed in a 324 cm^2 square with two parallel rigid boundaries (one fixed, one driven by a motor) and two passive lateral boundaries formed by a rubber band [33]. It can thus be deformed into a parallelogram at constant area to apply pure shear cycles with an amplitude much larger than the yield strain. For details see Refs. [5,33].

Cellular Potts model simulations [8,34] (Fig. 7) are fast, enabling us to scan a large range of disorders and accumulate statistics. They describe each bubble as a set of pixels, like in experimental images. Initially, we distribute at random $N = 112$ nine-pixel bubble seeds on a 200×200 pixel lattice. They are grown until they reach approximately the average bubble size $\langle A\rangle$, chosen to be 400 pixels. They are then randomly assigned target areas according to the desired area distribution. To shuffle the foam, we choose the effective temperature, and thus the amplitude of bubble edge fluctuations, high enough that T1s occur spontaneously [35]. The simulations are run for 2×10^6 Monte Carlo steps (MCSs), at which we checked that $\Delta n/\langle n\rangle$ reaches a steady value. Measurements presented here are averages over images in this steady regime.

SURFACE EVOLVER [36,37] simulations are more precise. They represent each side as an arc of a circle (Figs. 8 and 9); they provide detailed information about each bubble's position and shape. In our first set of data (hereafter "SE1"), already used in Ref. [19], each foam is prepared from a Voronoi construction based on seed points generated by a random Poisson point process [38,39], with the bubble areas adjusted to fit the desired area distribution where necessary, before convergence to an energy minimum. We cyclically shear, by deforming the shape of the periodic box, about four hundred foams with $N = 2500$ bubbles in two perpendicular directions with strain amplitude 1.5.

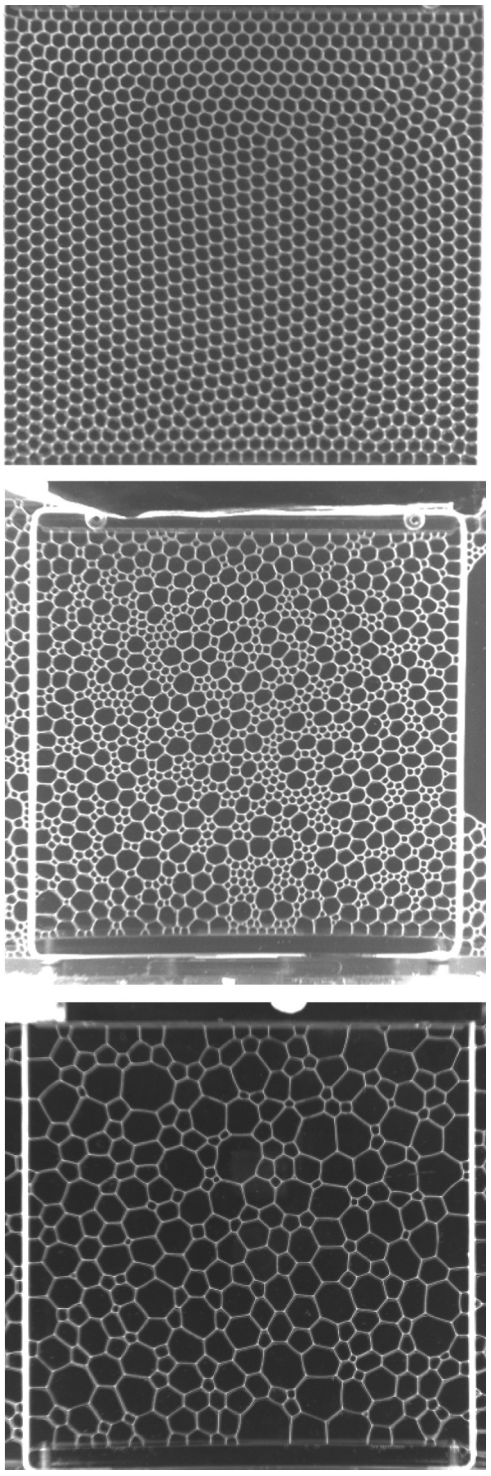

FIG. 6. Experiments: mono-, bi-, and polydisperse foams.

New SURFACE EVOLVER simulations (hereafter "SE2") were performed to create random 2D foams with very large polydispersity by adapting the methods of Kraynik, Reinelt, and van Swol [30,40] for modeling random three-dimensional (3D) foams. First, molecular dynamics was used to generate dense packings of rigid disks with densities ranging from 0.84 to 0.91. Then, Laguerre (weighted-Voronoi) tessellations were used to fill space with convex polygonal cells that enclose each

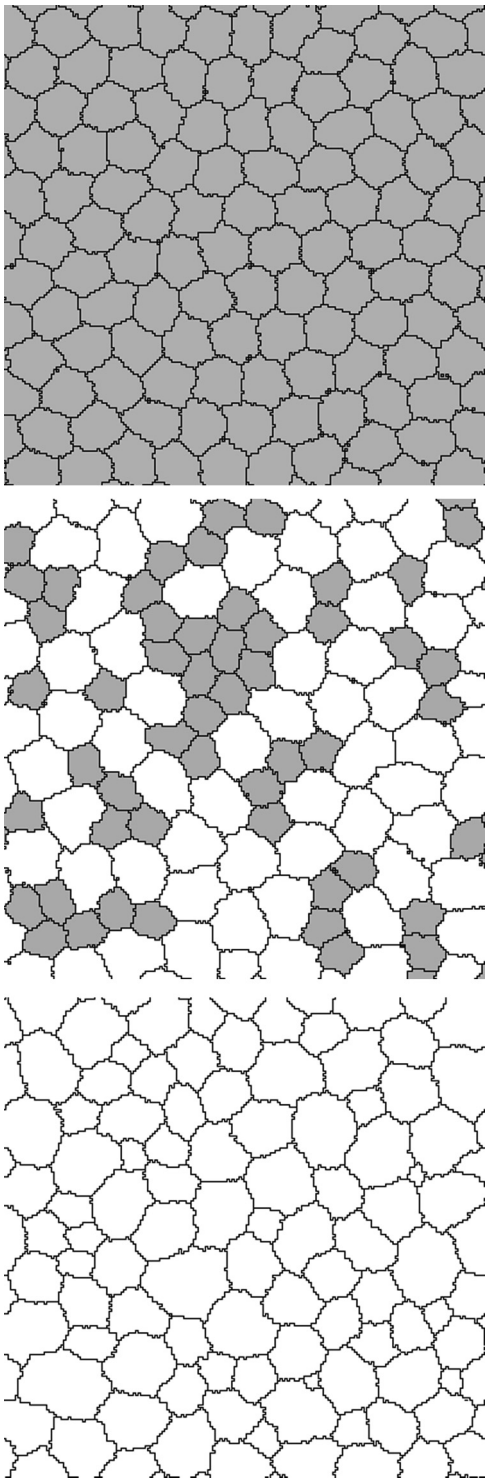

FIG. 7. Cellular Potts model simulations: mono-, bi-, and polydisperse foams. For the bidisperse foam, the population of small bubbles is highlighted.

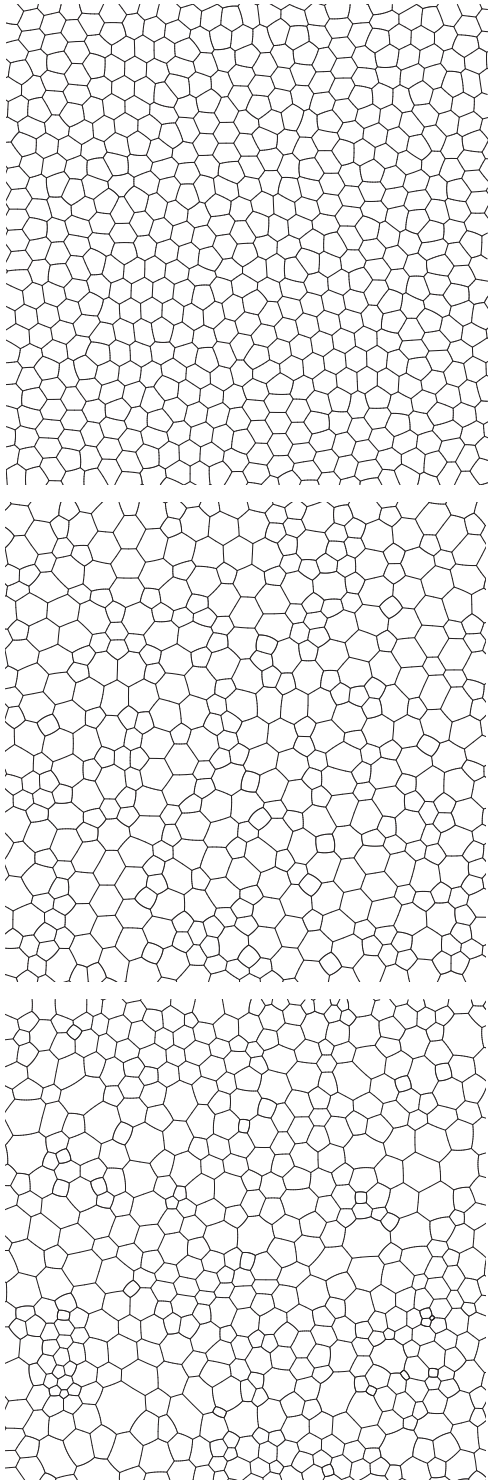

FIG. 8. SURFACE EVOLVER simulations SE1: mono-, bi-, and polydisperse foams.

disk and set the cell-area distribution. Foam polydispersity was controlled by using a lognormal distribution of the disk diameters, and varying the width of the distribution as well as the maximum diameter (to control the formation of extremely large cells). SURFACE EVOLVER [36,37] was then used to relax the Laguerre structures to satisfy Plateau's laws. In strong contrast to 3D simulations, the 2D relaxation process involved very few if any topological transitions that are triggered by cell edges shrinking to zero length. Consequently, the topological statistics of the Laguerre tessellations and fully relaxed foams are virtually identical. The foams were not shuffled. Finally, a slight distortion of the spatially periodic unit cell is performed until the stress becomes isotropic.

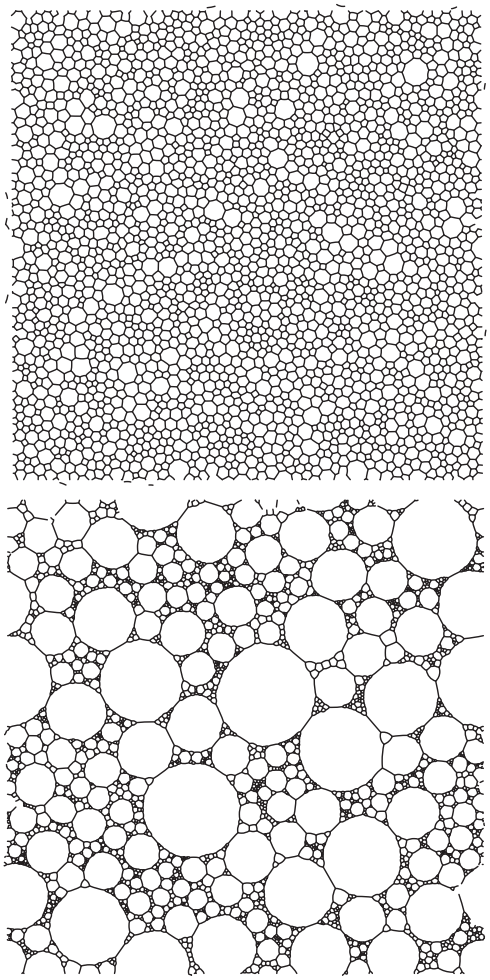

FIG. 9. SURFACE EVOLVER simulations SE2: foams with moderate and high polydispersities.

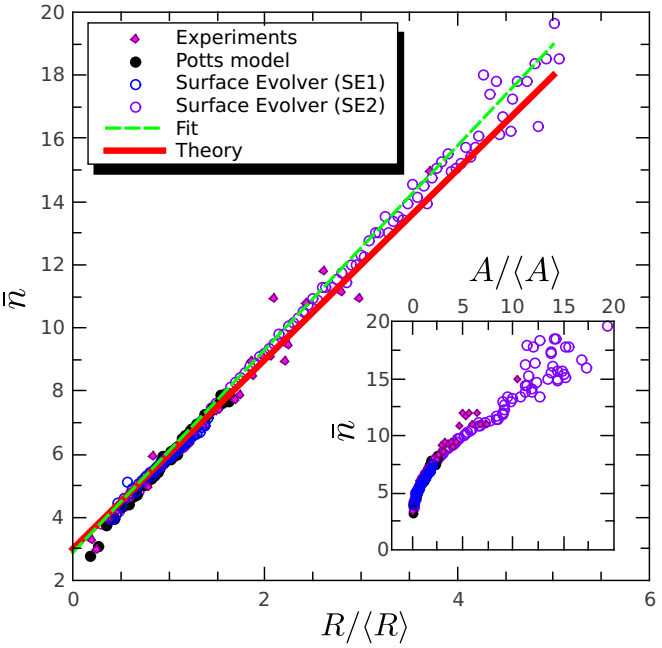

FIG. 10. (Color online) Average number of sides, $\bar{n}$, of a bubble vs its relative size $R/\langle R\rangle = \sqrt{A}/\langle\sqrt{A}\rangle$. This figure is the same as Fig. 2(a) of Ref. [19], with more data and larger polydispersities. Each foam contributes several points: two points for a bidisperse foam, more dispersed points for a polydisperse foam. Solid red line, Eq. (17); dashed green line, polynomial fit of degree 1 of the raw data: $\bar{n} - 6 = (3.22 \pm 0.02)(R/\langle R\rangle - 1)$. Inset: same data plotted vs $A/\langle A\rangle$, highlighting the nonlinear dependence of $\bar{n}$ on A.

These experiments and simulations show a linear correlation between the geometry and topology of individual bubbles, as predicted by Eq. (17), with a 7% difference in the slope (Fig. 10). They also successfully test the prediction of Eq. (19) (Fig. 11). Actually, the analytic approximation (19) seems to work far beyond its domain of validity (see Sec. III B). The comparison of the whole distributions of sides (see Fig. 12), rather than simply their second moments [41], shows that for slightly polydisperse foams [Fig. 12(a)], the agreement between the data and the model is extremely good. For larger dispersities [Fig. 12(b)], both the analytic approximation and the exact solution of the equations depart from the data as the size polydispersity increases. However, considering that our model has no adjustable parameters, and that SE2 foam samples are not shuffled, the shape and position of the distribution peaks are reasonably well predicted. The model could still be improved by revisiting the equiprobability hypothesis and/or the mean-field approximation [18].

V. LOW DISPERSITY LIMIT

At very low dispersity, we do not observe in experiments or in simulations the order-disorder transition predicted by our model. Although mean-field approximations are seldom

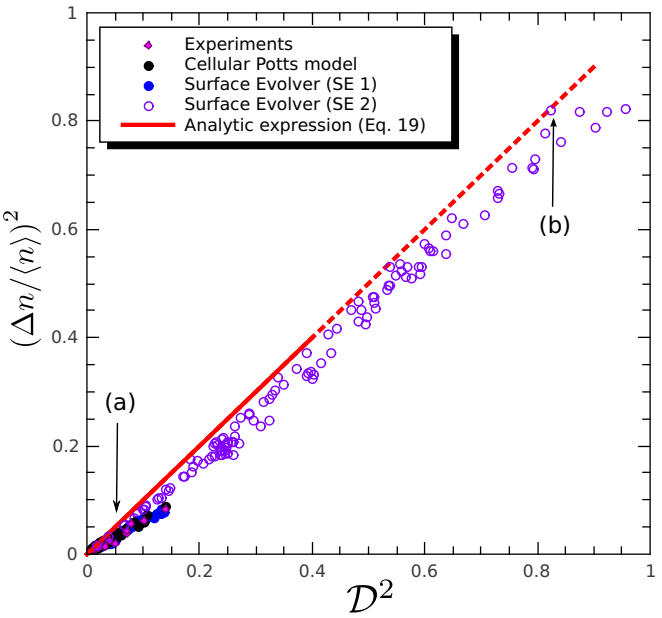

FIG. 11. (Color online) Test of Eq. (19) using experiments and simulations. Abscissa is the rhs of Eq. (19), defined in Eqs. (20) and (21). Each point represents a foam. Solid red line, expected range of validity of the analytic approximation [Eq. (19)]. The distributions of sides of the two foams indicated with arrows on the graph are shown in Fig. 12.

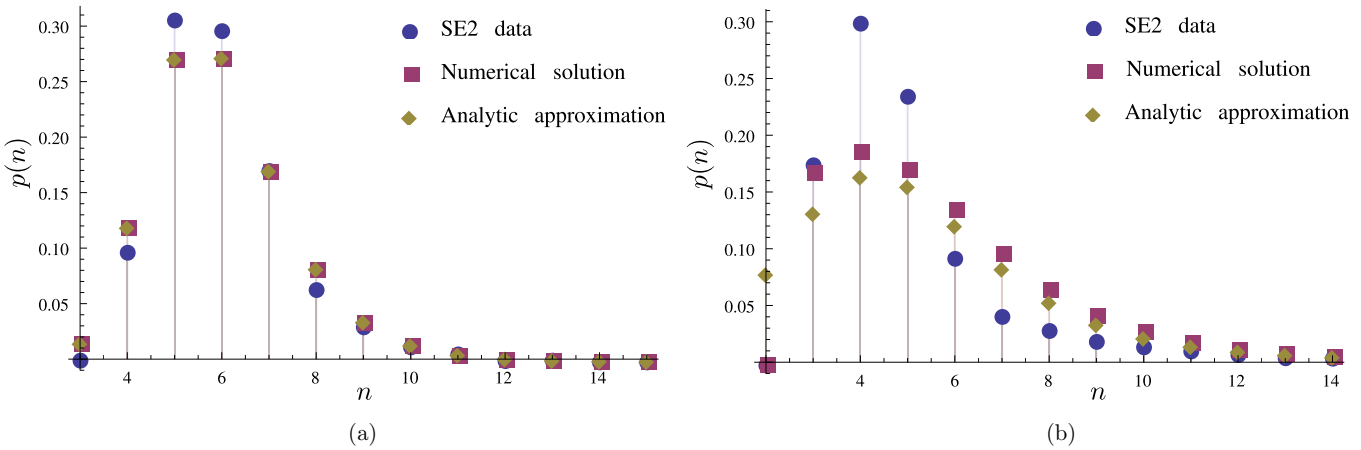

FIG. 12. (Color online) Comparison of the distribution of sides, $p(n)$, obtained from SURFACE EVOLVER (SE2) simulations (blue dots), exact resolution of the model [Eqs. (4)–(8)] (purple squares), and its analytic approximation [Eqs. (15) and (16)] (yellow diamonds): (a) narrow distribution $\mathcal{D}^2 = 0.0648$, $(\Delta n/\langle n\rangle)^2_{\text{model}} = 0.0648$, $(\Delta n/\langle n\rangle)^2_{\text{SE2}} = 0.0554$; (b) wide distribution $\mathcal{D}^2 = 0.8209$, $(\Delta n/\langle n\rangle)^2_{\text{model}} = 0.8208$, $(\Delta n/\langle n\rangle)^2_{\text{SE2}} = 0.8216$.

adapted to provide a good description of phase transitions, there are several possible reasons why this transition is not clearly observed in simulations and experiments. First, unlike simulations, which can use periodic boundary conditions (or boxes with sides meeting at $\pi/3$ or $2\pi/3$ angles, such as triangular or hexagonal boxes), experiments usually have rectangular or square boundaries, which are incompatible with a honeycomb pattern. Since each boundary locally orients the honeycomb lattice, in a rectangular box there are at least two perpendicular orientations of the honeycomb, resulting in at least two grain boundaries with length of order $N^{1/2}$. Topological considerations [42] imply a minimal number of paired five- and seven-sided bubbles per unit line of grain boundaries: the topological disorder is at least of order $3^{-9/8}2^{-1/4}N^{-1/4}$ [5].

Second, when the density of defects decreases, bubbles with five and seven sides tend to appear in pairs, surrounded by a large sea of six-sided bubbles [8]. Two 5-7 pairs can disappear if they get close together, in an opposite direction, to form a 5-7-7-5 quadrupole, that can be transformed into four six-sided bubbles by a T1 process. At decreasing defect density, it can take an increasingly large experiment or simulation time to obtain such low-probability T1 events. Thus, in practice, even with a very monodisperse foam, if we start from a disordered configuration and shuffle it during a finite time, we seldom reach more than 90% hexagons; this means 5% pentagons, 5% heptagons, and thus $\Delta n/\langle n\rangle \approx 5\%$. Better ordering requires special care during the foam preparation. In must be also emphasized that, for the new set of data (SE2) presented here, foams are not shuffled; hence we do not expect to see crystallization here.

Both above effects imply a finite topological disorder even at vanishing geometrical disorder: bubbles of the same size are not all hexagons. Corresponding points would be *above* the $y = x$ line in the graph of Fig. 3. Both are practical limitations and are not considered in our statistical model of perfectly shuffled foams.

VI. CONCLUSION

In summary, we have implemented a theoretical method to correlate geometrical and topological disorder in 2D liquid foams with low liquid content. We have identified the relevant parameters and variables, including a parameter $\mathcal{D}$ characterizing the geometrical disorder. We have then written equations based on classical statistical mechanics, solved them with controlled approximations tested numerically, and compared them to experiments and simulations. In particular we have shown that the model works even at extreme (high or low) dispersities, which had not been fully treated previously. This enables us to predict that a bidisperse foam crystallizes when the ratio of bubble radii is 1.4, irrespective of the proportion of small bubbles. Whereas hard disks crystallize around 1.2, due to the deformability of the bubbles, foams can crystallize over a larger range of size dispersities. Our method might be extended to various patterns and to higher dimensions.

ACKNOWLEDGMENTS

J.K. thanks A.F.M. Marée for help with the Potts simulations. A.M.K. thanks P. Grassia, G. Schroeder-Turk, and K. Mecke for their hospitality. S.C. thanks the FP7 IAPP project HYDROFRAC (Grant No. PIAP-GA-2009-251475) for funding. S.C. and A.M.K. acknowledge financial support from the Royal Academy of Engineering Distinguished Visiting Fellowship Scheme, and hospitality from S. Neethling. F.v.S. is supported by the United States Department of Energy, Office of Basic Energy Sciences, Division of Materials Sciences and Engineering. M.D., C.Q., and F.G. have belonged to the CNRS consortium "Foams and Emulsions," F.G. and J.K. to the CNRS consortium "CellTis," and M.D. to the CNRS consortium "MePhy."

[1] S. Hutzler and D. Weaire, *Physics of Foams* (Oxford University Press, Oxford, 1999).

[2] I. Cantat, S. Cohen-Addad, F. Elias, F. Graner, R. Höhler, O. Pitois, F. Rouyer, and A. Saint-Jalmes, in *Foams: Structure and Dynamics*, edited by S. J. Cox (Oxford University Press, Oxford, 2013).

[3] N. Kruyt, Int. J. Solids Struct. **40**, 511 (2003).

[4] J. Duplat, B. Bossa, and E. Villermaux, J. Fluid Mech. **673**, 147 (2011).

[5] C. Quilliet, S. Ataei Talebi, D. Rabaud, J. Käfer, S. J. Cox, and F. Graner, Philos. Mag. Lett. **88**, 651 (2008).

[6] K. A. Newhall, L. L. Pontani, I. Jorjadze, S. Hilgenfeldt, and J. Brujic, Phys. Rev. Lett. **108**, 268001 (2012).

[7] M. A. Fortes and P. I. C. Teixeira, J. Phys. A: Math. Gen. **36**, 5161 (2003).

[8] F. Graner, Y. Jiang, E. Janiaud, and C. Flament, Phys. Rev. E **63**, 011402 (2000).

[9] N. Rivier, in *Disorder and Granular Media*, edited by D. Bideau and A. Hansen (Elsevier, New York, 1993), p. 55.

[10] N. Rivier, in *Foams and Emulsions: Proceedings of 1997 Summer School, Cargèse, France*, edited by J.-F. Sadoc and N. Rivier, Nato ASI Ser. E (Kluwer, Dordrecht, 1999), p. 105.

[11] G. Schliecker and S. Klapp, Europhys. Lett. **48**, 122 (1999).

[12] C. Sire and M. Seul, J. Phys. I **5**, 97 (1995).

[13] C. Godrèche, I. Kostov, and I. Yekutieli, Phys. Rev. Lett. **69**, 2674 (1992).

[14] R. Blumenfeld and S. F. Edwards, Phys. Rev. Lett. **90**, 114303 (2003).

[15] A. Hocevar and P. Ziherl, Phys. Rev. E **80**, 011904 (2009).

[16] R. M. C. de Almeida and J. R. Iglesias, J. Phys. A **21**, 3365 (1988); J. R. Iglesias and R. M. C. de Almeida, Phys. Rev. A **43**, 2763 (1991).

[17] M. P. Miklius and S. Hilgenfeldt, Phys. Rev. Lett. **108**, 015502 (2012)

[18] M. Durand, Europhys. Lett. **90**, 60002 (2010).

[19] M. Durand, J. Käfer, C. Quilliet, S. Cox, S. A. Talebi, and F. Graner, Phys. Rev. Lett. **107**, 168304 (2011).

[20] J. A. F. Plateau, *Statique expérimentale et théorique des liquides soumis aux seules forces moléculaires* (Gauthier-Villars, Paris, 1873).

[21] D. A. Aboav, Metallography **3**, 383 (1970).

[22] C. B. O'Donovan, E. I. Corwin, and M. E. Möbius, Philos. Mag. **93**, 4030 (2013).

[23] A. E. Roth, C. D. Jones, and D. J. Durian, Phys. Rev. E **87**, 042304 (2013).

[24] D. Weaire and N. Rivier, Contemp. Phys. **25**, 59 (1984).

[25] W. C. Graustein, Ann. Math. **32**, 149 (1931).

[26] F. Reif, *Fundamentals of Statistical and Thermal Physics* (Waveland Press, Long Grove, IL, 2008).

[27] T. Aste and D. Sherrington, J. Phys. A: Math. Gen. **32**, 7049 (1999).

[28] T. Hamanaka and A. Onuki, Phys. Rev. E **75**, 041503 (2007).

[29] S. J. Cox and F. Graner, Phys. Rev. E **69**, 031409 (2004).

[30] A. M. Kraynik, D. A. Reinelt, and F. van Swol, Phys. Rev. E **67**, 031403 (2003).

[31] C. Raufaste, S. J. Cox, P. Marmottant, and F. Graner, Phys. Rev. E **81**, 031404 (2010).

[32] A. Abd el Kader and J. C. Earnshaw, Phys. Rev. Lett. **82**, 2610 (1999).

[33] C. Quilliet, M. Idiart, B. Dollet, L. Berthier, and A. Yekini, Colloids Surf. A **263**, 95 (2005).

[34] D. J. Srolovitz, M. P. Anderson, G. S. Grest, and P. S. Sahni, Scr. Metall. **17**, 241 (1983).

[35] P. Marmottant *et al.*, Proc. Natl. Acad. Sci. USA **106**, 17271 (2009).

[36] K. Brakke, Exp. Math. **1**, 141 (1992).

[37] http://www.susqu.edu/brakke/evolver/evolver.html

[38] http://www.susqu.edu/brakke/papers/voronoi.htm

[39] S. J. Cox and E. L. Whittick, Eur. Phys. J. E **21**, 49 (2006).

[40] A. M. Kraynik, D. A. Reinelt, and F. van Swol, Phys. Rev. Lett. **93**, 208301 (2004).

[41] For skewed distributions such as those shown in Fig. 12, the second moment Δn cannot be interpreted as the width of the distribution. That is why the distributions obtained with SE2 simulations look narrower but have a smaller topological disorder value $\Delta n/\langle n\rangle$ than the distributions derived from the model and its analytic approximation.

[42] L. Alfonso, M. E. Rosa, and M. A. Fortes, Coll. Surf. A **309**, 38 (2007).